Article

SOURCE DATA | TRANSPARENT PROCESS

THE EMBO JOURNAL

Crystal structures of the structure-selective nuclease Mus81-Eme1 bound to flap DNA substrates

Gwang Hyeon Gwon[1], Aera Jo[1], Kyuwon Baek[1], Kyeong Sik Jin[2], Yaoyao Fu[1], Jong-Bong Lee[3], YoungChang Kim[4] & Yunje Cho[1*]

Abstract

The Mus81-Eme1 complex is a structure-selective endonuclease with a critical role in the resolution of recombination intermediates during DNA repair after interstrand cross-links, replication fork collapse, or double-strand breaks. To explain the molecular basis of 3′ flap substrate recognition and cleavage mechanism by Mus81-Eme1, we determined crystal structures of human Mus81-Eme1 bound to various flap DNA substrates. Mus81-Eme1 undergoes gross substrate-induced conformational changes that reveal two key features: (i) a hydrophobic wedge of Mus81 that separates pre- and post-nick duplex DNA and (ii) a 5′ end binding pocket that hosts the 5′ nicked end of post-nick DNA. These features are crucial for comprehensive protein-DNA interaction, sharp bending of the 3′ flap DNA substrate, and incision strand placement at the active site. While Mus81-Eme1 unexpectedly shares several common features with members of the 5′ flap nuclease family, the combined structural, biochemical, and biophysical analyses explain why Mus81-Eme1 preferentially cleaves 3′ flap DNA substrates with 5′ nicked ends.

Keywords crystal structure; flap DNA; homologous recombination; interstrand cross-link repair; Mus81

Subject Categories DNA Replication, Repair & Recombination; Structural Biology

DOI 10.1002/embj.201487820 | Received 3 January 2014 | Revised 12 March 2014 | Accepted 18 March 2014 | Published online 14 April 2014

The EMBO Journal (2014) 33: 1061–1072

Introduction

Homologous recombination (HR) represents a major pathway for repairing double-strand breaks, damaged replication forks, and chromosome segregation (reviewed in Deans & West, 2011; Schwartz & Heyer, 2011). HR process leads to the formation of joint molecules (JMs) including Holliday junctions (HJs) that can be "dissolved" by the Bloom (BLM)-TopoIIIa-RMI1/2 (Sgs1-Top3-Rmi1/2 in yeast) helicase-topoisomerase complex or "resolved" by a set of structure-selective endonucleases including Mus81-Eme1 (Mms4), Slx1-Slx4, and Gen1 (Constantinou *et al*, 2002; Wu & Hickson, 2003; Ciccia *et al*, 2008; Ip *et al*, 2008; Fekairi *et al*, 2009; Muñoz *et al*, 2009; Svendsen *et al* 2009; Cejka *et al*, 2010).

The Mus81-Eme1 nuclease plays critical roles in resolving JM intermediates during the repair of internal cross-links and replication fork collapse in mitotic cells and in meiotic cross-overs (Boddy *et al*, 2001; Chen *et al*, 2001; Doe *et al*, 2002; Hanada *et al*, 2006, 2007). Yeast and metazoan mus81- or mms4/eme1-deficient mutants have been shown to exhibit hypersensitivity to a variety of DNA-cross-linking agents (Interthal & Heyer, 2000; Dendouga *et al*, 2005). Mus81-Eme1 with the help of ERCC1 resolves incompletely replicated intermediates at common fragile sites and separates sister chromatids during early mitosis (Naim *et al*, 2013; Ying *et al*, 2013). Loss of Mus81 or Eme1/MMS4 significantly increases the number of gross chromosomal arrangements during normal cell division (Abraham *et al*, 2003; Dendouga *et al*, 2005; Hiyama *et al*, 2006; Wechsler *et al*, 2011).

The Mus81-Eme1 complex is a member of the MUS/XPF endonuclease family (reviewed in Hollingsworth & Brill, 2004; Ciccia *et al*, 2008; Schwartz & Heyer, 2011). Earlier studies report that Mus81-Eme1 resolves intact HJs through a nick-and-counternick mechanism (Gaillard *et al*, 2003). However, Mus81-Eme1 does not efficiently cleave intact HJs *in vitro*. Instead, Mus81-Eme1 preferentially cleaves nicked JMs including 3′ flap, replication fork (RF), and nicked HJs *in vitro* (Doe *et al*, 2002; Whitby *et al*, 2003; Fricke *et al*, 2005; Chang *et al*, 2008; Ehmsen & Heyer 2008). Recent studies have shown that Slx1-Slx4 initially cuts a junction of intact HJ, followed by the second incision on the opposite junction by Mus81-Eme1 to generate linear duplex DNA products (Castor *et al*, 2013; Garner *et al*, 2013; Wyatt *et al*, 2013).

Despite extensive structural and biochemical studies, it is unclear how MUS/XPF family nucleases recognize and resolve their

1 Department of Life Science, Pohang University of Science and Technology, Pohang, South Korea
2 Pohang Accelerator Laboratory, Pohang University of Science and Technology, Pohang, South Korea
3 Department of Physics, Pohang University of Science and Technology, Pohang, South Korea
4 Biosciences Division, Structural Biology Center, Argonne National Laboratory, Argonne, IL, USA
*Corresponding author. Tel: +82 54 279 2288; Fax: +82 54 279 8111; E-mail: yunje@postech.ac.kr

substrates at the molecular level (Newman *et al*, 2005; Nishino *et al*, 2005; Roberts and White 2005; Tsodikov *et al*, 2005; Chang *et al*, 2008). Crystal structure of DNA-free Mus81-Eme1 revealed that Mus81-Eme1 consists of the nuclease domain formed by Mus81 nuclease and Eme1 nuclease-like domain, and two HhH2 from hMus81 and hEme1 ("MHhH2" and "EHhH2") that we refer to as the 2HhH2 domain (Chang *et al*, 2008). Previous studies of Mus81-Eme1 and its family members suggest that both MHhH2 and EHhH2 domains of Mus81-Eme1 are involved in binding to DNA substrates (Newman *et al*, 2005; Nishino *et al*, 2005; Chang *et al*, 2008). However, these studies do not provide information of (i) how Mus81-Eme1 recognizes and cleaves its substrate, (ii) the molecular determinant of the substrate preference by Mus81-Eme1, (iii) how Mus81-Eme1 determines the incision site(s), and (iv) biological implications of the protein-DNA interaction.

To address these questions, we performed structural studies of human Mus81-Eme1 with three different flap substrates. We show that DNA binding induced significant conformational changes in the linkers connecting the nuclease and HhH2 domains of Mus81 and Eme1, which transforms the Mus81-Eme1 structure from a compact to an open state. These changes unmask the hydrophobic wedge and create the 5′ end binding pocket facilitating the DNA substrate bending by Mus81-Eme1, ultimately place the incision strand at an active site of Mus81. These features explain why Mus81-Eme1 selects 3′ flap DNA over 5′ flap DNA and processes the 5′ nicked DNA substrates more efficiently. Unexpectedly, we found that hMus81-Eme1 shares several key structural features with 5′ flap nucleases including core motif, hydrophobic wedge, 5′ end binding pocket, and DNA kinking, implicating that the structures and functions are conserved in the flap nuclease family.

Results

Structure determination

To characterize structural mechanism by which Mus81-Eme1 recognizes and resolves its substrates, we crystallized human Mus81 (ΔN245)-Eme1 (ΔN177) bound to three different DNA substrates. This N-terminal truncated Mus81-Eme1 construct showed identical catalytic activities for various substrates compared to the full-length human Mus81-Eme1 (Chang *et al*, 2008); hence, we hereafter refer this construct as hMus81-Eme1. Initially, we obtained the crystal ($P2_12_12$ space group) in the presence of 17-bp dsDNA with 5-nt 5′ flap (crystal I). The 2.8 Å structure of the crystal clearly revealed the presence of DNA and the substrate-induced conformational changes in hMus81-Eme1. However, in this crystal, Mus81-Eme1 and DNA were bound as a catalytically inactive complex because the 5′ flap DNA formed a duplex DNA with a disordered 5′ flap. This conformation of DNA mimics the post-nick duplex of the DNA

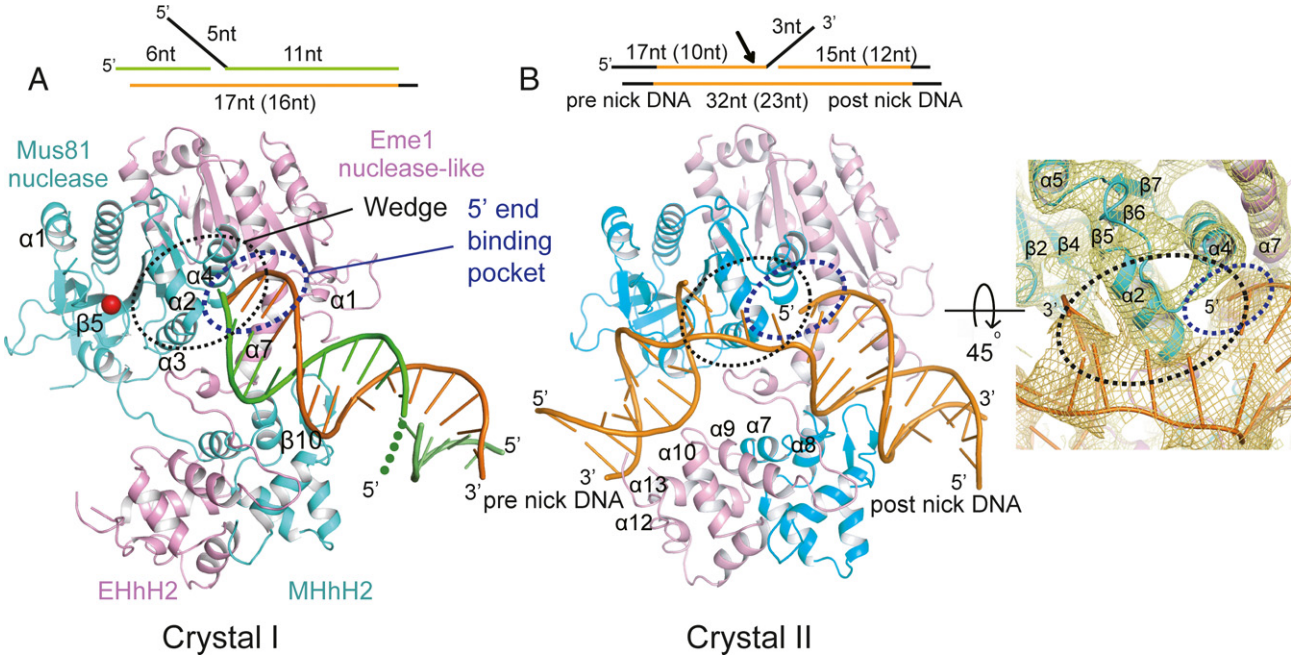

Figure 1. Overall structure of the hMus81-Eme1-DNA complex.

A A complex structure (crystal I) containing hMus81 (cyan)-Eme1 (pink) bound to a 5′ flap DNA. The nuclease and nuclease-like domains are on top of the EHhH2 and MHhH2 domains, respectively. Each strand of a duplex DNA is shown with green and orange backbone. The wedge (black dotted circle) corresponds to helix α2-turn-helix-α3 and loop β6-α4. The "5′ end binding pocket" is shown with blue dotted circle. Disordered 5′ flap part is marked with orange dots.

B Left: A hMus81 (cyan)-Eme1 (pink) structure bound to a 3′ flap DNA (crystal II) is shown in the same orientation as in (A). A schematic diagram for a substrate is shown on top. The approximate cleavage site is marked with an arrow and size of the crystallized DNA (black) is shown. Size of modeled DNA (orange) is shown inside the parentheses. Right: the 6.5 Å 2Fo-Fc map was calculated with phases after the model with the omitted DNA was subjected to simulated annealing refinement. Contoured at 1.0 σ. On the right and left of the wedge, the post-nick and the pre-nick DNA are placed, respectively.

substrates in other catalytically active crystal forms (see below, Fig 1A). To examine whether the structural transition observed in crystal represents true conformational change in response to the substrate binding, we further pursued to obtain other crystals using different DNA substrates. After extensive trials, we successfully grew two additional crystals with different 3′ flap DNA, one of the best *in vitro* substrates (Supplementary Table S1). We obtained two different complex crystals: one with a 32-bp dsDNA with 3-nt 3′ flap (crystal II; C2, 6.5 Å) and another complex crystal with a 24-bp dsDNA with 3-nt 3′ flap (crystal III; $C222_1$, 6.0 Å) (Supplementary Materials and Methods and Supplementary Fig S1A). Although these crystals diffracted to limited resolution, electron density maps clearly provided features of overall conformations of Mus81-Eme1 and 3′ flap DNA (Fig 1B and Supplementary Fig S1A).

Crystals I, II, and III contain one, two, and four hMus81-Eme1-DNA complexes in the asymmetric unit, respectively. Seven Mus81-Eme1-DNA structures show similar overall structures, but 2HhH2 position relative to the nuclease domain is variable in some structures. For example, four Mus81-Eme1 complexes in crystal III exhibit slightly different rigid body position of the 2HhH2 domain (Supplementary Fig S1B and C). The overall structure of the Mus81-Eme1 complex in crystal I is very similar to one of the complexes in crystal III. Furthermore, the overall structure of the complex in crystal II is close to another one of the complexes in crystal III.

Although crystal packing may contribute to the positional differences in 2HhH2, intrinsic malleability of the linker between the nuclease and HhH2 domains may be a major factor determining this difference (see below). All of our DNA-bound structures are substantially different from the structure of DNA-free human Mus81-human Eme1 (PDB ID: 2ZIX) or zebra fish Mus81-human Eme1 (zfMus81-Eme1, 2ZIU), suggesting that DNA binding induced notable conformational changes in Mus81-Eme1.

Overview of the human Mus81-Eme1 structure

Because the overall structures are more or less similar across seven structures, we will primarily describe the structural features and conformational changes in crystal I (2.8 Å) in detail, where a bound DNA corresponds to the post-nick duplex of a 3′ flap DNA. We will also partly describe the gross features of crystals II (6.5 Å) and III (6.0 Å). Pre-nick duplex DNA is packed between the EHhH2 and the Mus81 nuclease domain, whereas the post-nick duplex DNA is primarily bound to the Eme1 nuclease-like domain and MHhH2 domain (Fig 1A and B). The interface between the pre- and post-nick DNA is bent approximately by 100° and formed by four-nt single-stranded (ss) DNA (crystal II). The pre- and post-nick duplexes are separated by the hydrophobic wedge formed by helix-turn-helix (HTH, α2-α3) and loop β6-α4 of Mus81. On the right side of the wedge, a pocket (we refer "5′ end binding pocket") formed by the nuclease (α2 to α4) of Mus81 and the Eme1 linker (α7) interact with the 5′ nicked end of post-nick duplex (Fig 1B). On the left side of the wedge, the 3′ end of the pre-nick DNA is directed to the active site (α1 and α2, and loop β3-β4). In the DNA-bound structure, hMus81 linker (residues 464–470) becomes linearly extended and hEme1 linker (residues 445–472) forms an ordered structure, which separates the nuclease and the 2HhH2 domains, leading to an open and relaxed overall conformation compared to the compact form of DNA-unbound Mus81-Eme1 (Fig 2A and B).

The substrate-induced structural transition of hMus81-Eme1

Although DNA-free zfMus81-hEme1 structure (2ZIU, 2.8 Å) was determined at a higher resolution than that of hMus81-hEme1 (2ZIX, 3.3 Å), both structures are very similar (Chang *et al*, 2008). Thus, we compare human DNA-free and DNA-bound Mus81-Eme1 crystal structures for consistency. Comparison result between human DNA-free and DNA-bound Mus81-Eme1 structures is virtually identical to that between DNA-free zfMus81-hEme1 and DNA-bound hMus81-Eme1. Overall, the substrate binding rotates the 2HhH2 domain by 40° relative to the nuclease domain (Fig 2A and B). The most striking conformational change occurs in Eme1 linker (residues 445–472). The disordered loop (residues 445–455) becomes ordered and extends the five-turn helix (α7) to a continuous and kinked (at Pro447) eight-turn helix (Fig 2A–D). This region contains Lys441 and Lys449 that interact with the 5′ terminal nts of 5′ flap DNA (or the 5′ nicked end of the post-nick duplex in 3′ flap DNA) (Figs 2D, 3A and Supplementary Fig S2). Thus, we presume that binding of the 5′ nicked end of the post-nick DNA to these residues initiates structural rearrangement.

This "disorder-to-order" transition of the hEme1 linker is important for the following several reasons. First, it alters the orientation and conformation of loops α7-α8 and α8-α9 of Eme1, which results in disclosure of the wedge (HTH (α2-α3) and loop β6-α4) of hMus81 and formation of the "5′ end binding pocket" (Fig 2B and D, Supplementary Movie S1). In DNA-free hMus81-Eme1, Trp465 in loop α8-α9 of Eme1 is packed against residues from the wedge and the "5′ end pocket" of Mus81 and interferes the substrate binding. These residues include Ile344, Phe349, Arg350, Thr383, Ala387, and Asn390 of hMus81 (Fig 2C). The substrate binding relocates the loops α7-α8 and α8-α9 as much as 30 Å and flips Trp465 to interact with MHhH2 to open the wedge and to create the pocket. Here, Trp465 interacts with Arg477, Met480, and Gln481 of MHhH2 and packed by Phe459, Ala466, and Gln488 of EHhH2 (Fig 2D). Second, loops α7-α8 and α8-α9 of Eme1 are directed to hMus81 linker and alter the structure of hMus81 linker, shifting it toward Mus81 nuclease domain as much as 14 Å. Third, the structural transition of these linkers ultimately rotates the 2HhH2 domain by 40° (20 Å), which is stabilized through interactions between the hairpin β10-β11 of Mus81 and helix α1 of Eme1 (Figs 1B, 2B and D). These conformational changes allow EHhH2 and MHhH2 to interact with pre- and post-nick DNA, respectively, and force the flap substrate DNA to kink with the aid of the wedge. Such sharp DNA bending would not occur in the DNA-free closed state primarily because the wedge is completely buried by 2HhH2; hence, the "5′ end binding pocket" cannot form in full shape.

The post-nick DNA-binding region

As we observed in the structure of crystal I, post-nick DNA binding is sufficient to induce conformational changes in Mus81-Eme1, suggesting that this part of the substrate initially interacts with the nuclease (Figs 1A, 2B and D). Interactions between hMus81-Eme1 and post-nick DNA are best described in two parts (crystal I). The first is the minor groove contact near the center of post-nick DNA by helix α1 of Eme1 and loops α7-α8 and β10-β11 of MHhH2 (Fig 3B, Supplementary Figs S2 and S3). Arg483, Ser486, and Lys489 of Mus81 interact with the phosphate oxygen atoms of Cyt5′,

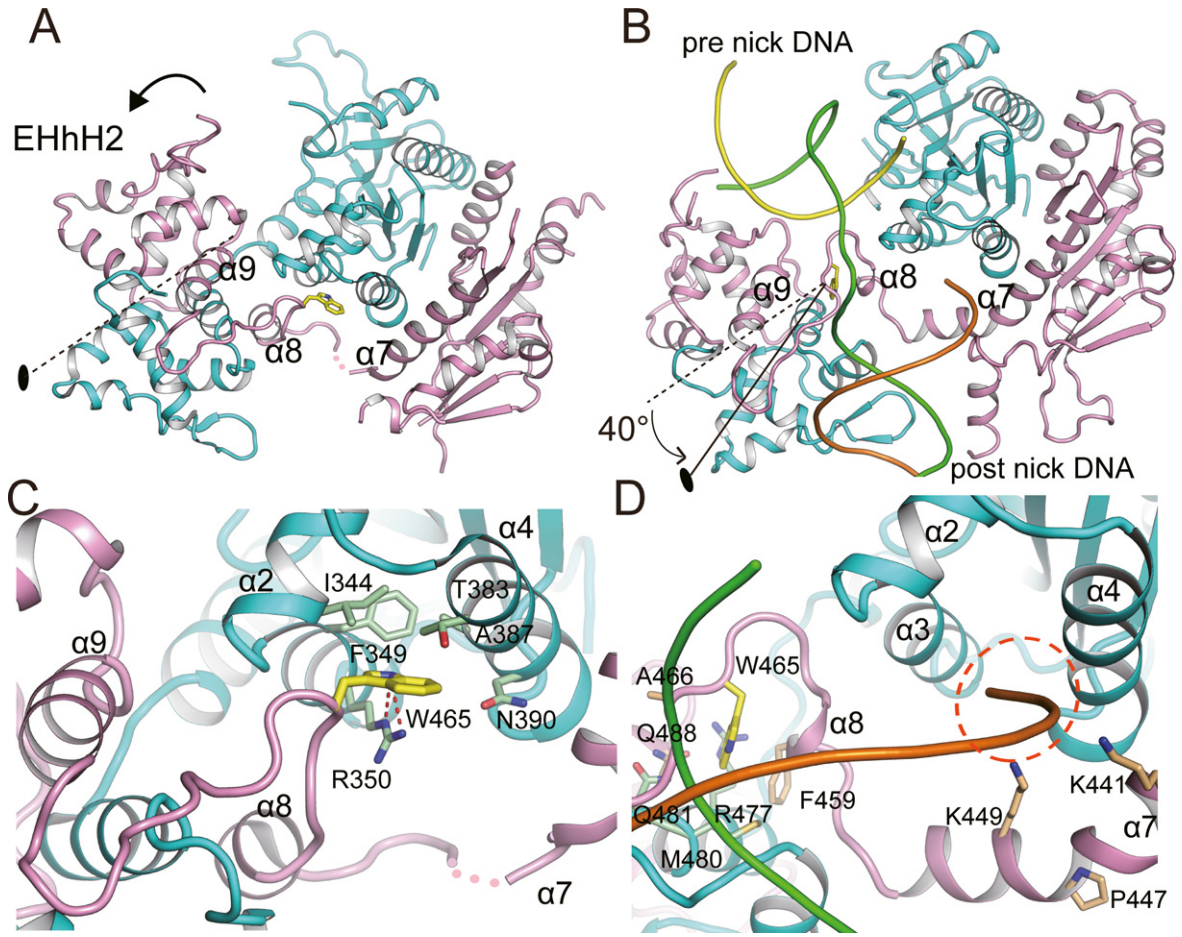

Figure 2. DNA-induced conformational changes in hMus81-Eme1.

A Overall structure of DNA-unbound hMus81 (cyan)-hEme1 (pink). An arrow indicates the rotation of the 2HhH2 domain.

B Overall structure of DNA-bound hMus81-Eme1. DNA binding extends the hMus81 and hEme1 linkers and opens the interface between the nuclease: nuclease-like and 2HhH2 domains. A central axis at the interface of MHhH2 and EHhH2 is rotated by 40° in the presence of DNA. For more accurate comparison, structure of crystal I is drawn. The pre-nick duplex is added from the crystal II after superposition. The root mean square deviation value for the Cα atoms of the nuclease and 2HhH2 domain between DNA-free and DNA-bound Mus81-Eme1 is 1.4 Å and 1.6 Å, respectively.

C Close-up view of the Eme1 linker in the DNA-free Mus81-Eme1 structure. Trp465 (yellow) is packed by hydrophobic residues (pale green) of Mus81 and blocks the wedge (α2-turn-α3).

D Close-up view of the Eme1 linker region in the DNA-bound open and relaxed state of hMus81-Eme1, in which Trp465 is flipped and interacts with residues from MHhH2 (pale green) and Eme1 (light orange; crystal I).

Ade6′, and Cyt7′ (crystal I; Fig 3B, top). In the opposite face, Lys241 and Arg244 (Eme1) form ion pairs with the phosphate oxygen atoms of Ade8′ (Fig 3B, bottom). The most critical feature is Arg530 from MHhH2, which deeply wedged into the Ade10′-Thy10 and Cyt9′-Gua9 base pairs at the minor groove (Fig 3B, middle).

To examine the significance of the interactions between MHhH2 and the minor groove, we replaced Arg530, Arg483, and Lys489 with alanine. The R530A and R483A/K489A/R530A mutant at MHhH2 exhibited decreased nuclease activities toward a nicked HJ. After 8 mins of reaction, the amount of cleaved nHJ substrate by the R530A and the R483A/K489A/R530A mutant was approximately 50% and 5% relative to the wild-type (WT) Mus81-Eme1, respectively. Although the measured points in time courses are not exactly linear, which makes it difficult to obtain an accurate quantification analysis, the results clearly suggest that these residues in the MHhH2 region are important in recognition and cleavage of DNA (Fig 3C and D, and Supplementary Table S2). More reduction in the nuclease activities toward 3′ flap DNA was observed for these mutant proteins (Fig 3G and H). Approximately 16% and 5% of the substrate cleavage were achieved by the R530A and the R483A/K489A/R530A mutant, respectively, relative to WT protein at 8 mins of reaction.

The second interaction occurs at the 5′ end binding pocket, where the two 5′ terminal nts of the 5′ flap DNA in crystal I corresponding to 5′ nicked end of the post-nick duplex of 3′ flap DNA in crystals II and III are involved in binding. The 5′ terminal end nt ("G1") of the 5′ flap DNA is disordered and not modeled. The next two nts fit tightly into the "5′ end binding pocket," and one of them ("A3") is unpaired (Fig 3A and E). In this pocket, the phosphate oxygen of Ade2 interacts with Arg350 (Mus81) and Lys449 (Eme1), and Ade2 base and sugar are surrounded by the residues from helix α7 in Eme1 and helix α4 and loop α4-β7 in Mus81; Ile344, Ile345,

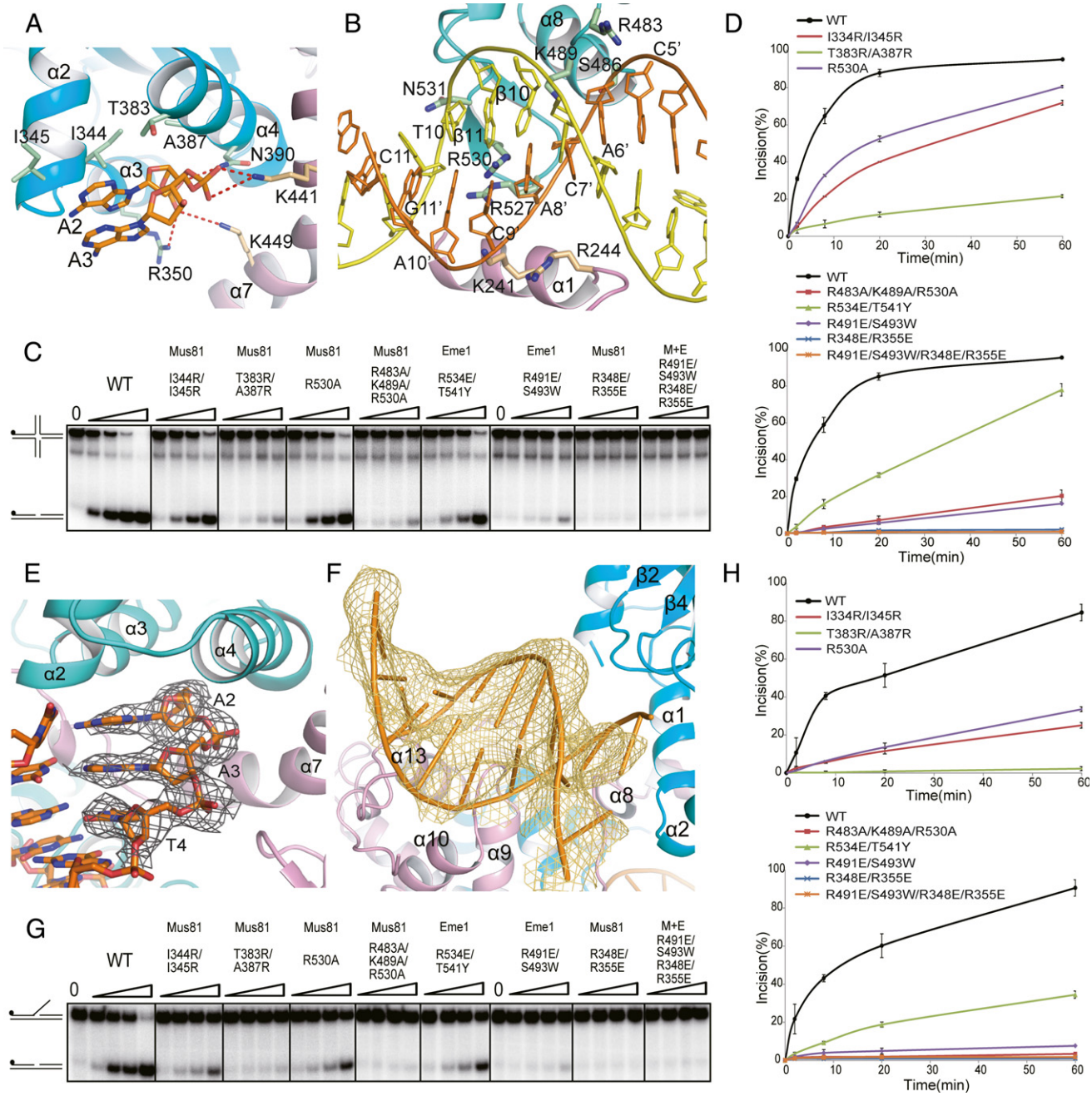

Figure 3. Interactions between the hMus81-Eme1 complex and DNA substrate.

A The 5′ of the nicked end bound to the "5′ end binding pocket". The two terminal phosphodiesters interact with Arg350 and Asn390 (Mus81, pale green) and Lys441 and Lys449 (Eme1, light orange), at the pocket (crystal I).

B The post-nick DNA binds to hMus81 (MHhH2) and Eme1 (nuclease-like domain). The interactions can be grouped into three regions; (top) Arg483, Ser486, and Lys489 interact with Cyt5′, Ade6′, and Cyt7′; (middle) Arg527 and Arg530 inserted into the minor groove; (bottom) Lys241 and Arg244 of Eme1 bind to Ade8′. Interactions are described based on the structure of crystal I.

C Nuclease activities of various hMus81-Eme1 mutants were examined toward a nicked HJ. Various hMus81-Eme1 proteins (2 nM) were incubated with a substrate DNA (20 nM) at 37°C for 2, 8, 20, and 60 min (see Supplementary Table S2).

D Quantification of the substrate cleavage is shown. Percentage of the cleaved DNA substrate after the reaction was quantified using phosphorimager analysis. The error bars are calculated from the standard deviation.

E A simulated annealing omit map (1.0 σ) of the 5′ end junction at the binding pocket at 2.8 Å resolution.

F The 6.0 Å electron density map for the pre-nick DNA bound to hMus81 (nuclease)-Eme1 (EHhH2) contoured at 2.5 σ (crystal III). The Fo-Fc map was calculated with phases after the model with the omitted pre-nick DNA was subjected to simulated annealing refinement.

G, H Nuclease activities of various hMus81-Eme1 mutants were examined toward a 3′ flap DNA and quantified. Assay conditions were same as those of (C) and (D).

Source data are available online for this figure.

and Thr383 of Mus81 surround the Ade2 base, and Phe349, Lys353, and Ala387 of Mus81 bind to Ade2 sugar (Fig 3A and Supplementary Fig S3).

We hypothesized that interactions in the 5′ end binding pocket are critical for the substrate selectivity, since this pocket can accommodate a 5′ nicked end of a 3′ flap DNA but not a long 5′ flap of the 5′ flap DNA (Fig 3A and E). To understand the significance of the wedge and 5′ binding pocket, we generated two double mutant proteins. We predicted that introduction of bulky residues to the 5′ end pocket should block the pocket and negatively affects the nuclease activity. Thus, we mutated Thr383 and Ala387 to arginine. The T383R/A387R mutant at the binding pocket cleaved only 10% and 0.5% of the nHJ and the flap substrate, respectively, relative to the WT Mus81-Eme1 after 8 mins of reaction (Fig 3C, D, G and H, and Supplementary Table S2). We also examined the importance of wedge by replacing Ile344 and Ile345 to arginine. The I344R/I345R mutant at the wedge cleaved about 33% of nHJ (14% of the flap DNA) substrate at 8 mins of the reaction (Fig 3C, D, G and H). Our mutational analysis could not differentiate whether the mutational effects are due to DNA binding or due to chemical step of catalysis. However, because we used an excess amount of the substrate relative to Mus81-Eme1, it is possible that DNA-binding affinities play a more important role for the observed mutational effects. Collectively, these results demonstrate the significance of the "5′ end binding pocket" and the wedge in substrate recognition and nuclease activity.

The pre-nick DNA-binding region

The EHhH2 domain binds to the pre-nick DNA in a twofold pseudo-symmetric manner to the interaction between MHhH2 and post-nick DNA (Figs 1B and 3F). Structural superposition of the 2.8 Å structure of crystal I into the 6.0 Å electron density map reveals that loops α9-α10 and α12-α13 of EHhH2 interact with the minor groove of the pre-nick DNA. Arg491 (α9-α10) and Arg534 (α12-α13) are likely to participate in recognizing the pre-nick DNA (Fig 3F, Supplementary Fig S2). We tested the significance of these interactions by mutational analyses. The R534E/T541Y (EHhH2) mutant cleaved approximately 25% nHJ substrate (25% flap DNA), while R491E/S493W mutant exhibited about 4% cleavage of nHJ relative to the WT Mus81-Eme1 after 8 mins of reaction (Fig 3C, D, G and H, and Supplementary Table S2).

In the opposite side, Mus81 nuclease domain binds to the minor groove through helix α3, loops β3-β4, α6-α7, and β2-α1 (Fig 3F). Several positively charged residues are clustered here: Arg348, Arg355, Lys302, and Lys465 (Supplementary Fig S2). The charge inversion mutation of Arg348 and Arg355 at helix α3 to glutamate almost completely abolished the nuclease activities toward nicked HJ and 3′ flap DNA substrates (Fig 3C, D, G and H, and Supplementary Table S2).

Mus81-Eme1 bends DNA to facilitate substrate recognition and cleavage

The interface between pre- and post-nick DNA of a 3′ flap substrate in Mus81-Eme1 is sharply kinked. To validate our structural observation, we performed fluorescence resonance energy transfer (FRET) analysis using 3′ flap DNA containing ends labeled with FAM and TAMRA (TMR, R_0 = 50 Å; Supplementary Fig S4A and B). The dual-labeled 3′ flap DNA substrate exhibited significant changes in the FRET signal intensities in the presence of hMus81-Eme1 compared to in the absence of nuclease, suggesting that Mus81-Eme1 brings the ends of pre- and post-nick DNA closer. In contrast, an addition of hMus81-Eme1 did not show any quenching on 26-mer dsDNA labeled with FAM-TMR (Supplementary Fig S4B). hMus81-Eme1 does not quench the donor- or acceptor-alone-labeled DNA, and the fluorescence intensity of substrates labeled with FAM or TMR remains constant independent of protein concentration. These FRET data suggest that the observed changes in the fluorescent intensities reflect changes in energy transfer caused by decreasing end-to-end distance (Supplementary Fig S4C and D). Collectively, FRET measurements show that hMus81-Eme1 significantly kinks the 3′ flap DNA conformation, supporting our crystal structures.

Active site

The DX_nERKX_3D sequence has been proposed to be the signature motif of the active site of MUS/XPF family members (Ciccia *et al*, 2008) (Supplementary Fig S2). Previous studies suggested that Asp307, Glu333, and Arg334 (carbonyl oxygen) of hMus81 are potential ligands for Mg^{2+} ion (Newman *et al*, 2005; Nishino *et al*, 2005; Chang *et al*, 2008). To identify the active site within hMus81, we soaked the crystal of the hMus81-Eme1-DNA complex (crystal I) in buffer containing 1 mM $MgCl_2$. The Fo-Fc map revealed strong density (over 5σ) where we placed a Mg^{2+} ion. This Mg^{2+} ion interacts with the carboxyl groups of conserved Asp274 (2.3 Å), Glu277 (2.3 Å), and Asp307 (2.2 Å), which are in close proximity to the signature motif (Fig 4A and Supplementary Fig S2). Mutation of Asp274, Glu277, or Asp307 to alanine almost completely abrogated the nuclease activities of Mus81-Eme1 toward a nicked HJ substrate (Fig 4B). The Mg^{2+} ion-binding site of Mus81 resembles a metal on the nucleophile side in nucleases or polymerases which employ two-metal-ion catalysis (Yang, 2008). However, we could not observe the electron density for additional Mg^{2+} ion. We presume that because hMus81-Eme1 and 5′ flap DNA in crystal I form a non-catalytic complex devoid of the pre-nick duplex, we were not able to observe the second metal ion, which may bind stably only in the presence of the substrate DNA. It has been reported that the binding of an additional metal ion can be unclear even in enzyme-substrate complexes (Yang *et al*, 2006; Freudenthal *et al*, 2013). We though predict that the second Mg^{2+} ion is located near Asp307 and Glu333 upon formation of the catalytic Mus81-Eme1-DNA complex.

When the 2.8 Å structure is superimposed to the 6.0 Å electron density map of crystal III (or the 6.5 Å map of crystal II), the electron density for the DNA backbone is directed to the active site and surrounded by several acidic residues from loops β2-α1 and β3-β4 and strand β5 (Fig 4C and Supplementary Fig S2). The closest DNA backbone is located about 4 Å away from the metal ion, which further confirms the active site of Mus81. We predict that this DNA trace represents the incision strand.

Mus81-Eme1 shares common structural features with 5′ flap nucleases

Mus81-Eme1 can be classified into a JM resolvase or a structure-selective nuclease (Chen *et al*, 2001; Hollingsworth & Brill, 2004).

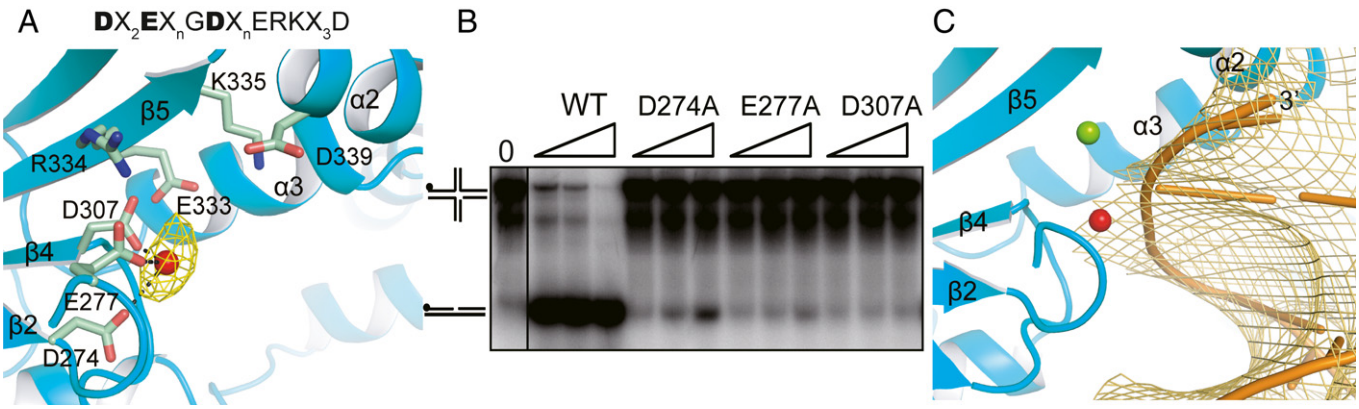

Figure 4. Structure and function of the active site residues of Mus81.

A In the active site of Mus81, Asp274, Glu277, and Asp307 are within 2.2 ~ 2.3 Å from the Mg^{2+} ion. A simulated annealing Fo-Fc omit map (5.0 σ) of a metal ion is shown at 2.8 Å resolution. Key residues are also displayed.

B Mutational analysis of the Mg^{2+}-interacting residues: Various concentrations (1, 2, and 5 nM) of WT hMus81-Eme1, D274A, E277A, or D307A were added to a nHJ DNA (20 nM) at 37°C for 60 min.

C The active site of Mus81 with the incised strand modeled in the 6.0 Å Fo-Fc electron density map drawn at 2.2 σ contour level (crystal III). The green-colored metal ion is modeled from the structures of archaeal and Xpf nucleases (Newman *et al*, 2005; Nishino *et al*, 2005), and the red colored metal ion is from the 2.8 Å structure of crystal I.

Source data are available online for this figure.

Structural analyses showed that the nuclease domain of Mus81 shares limited similarity with those of JM resolvases from bacteriophage and bacteria. Among the reported structures of the phage and bacterial JM resolvases, structure of T7 endonuclease 1 (T7 endo, 2PFJ) most closely resembles that of Mus81 (Hadden *et al*, 2007). Structure of T7 endo possesses a few helices and strands that can be superimposed to the helices (α3 to α5) and strands (β2 to β7) of Mus81. However, instead of a HTH motif of Mus81, the strand-turn-helix (equivalent to helix α3) separates the HJ arms in T7 endo, and no features like a pocket and the 2HhH2 domain of Mus81-Eme1 are observed. Structure of the *Thermus thermophilus* RuvC (*Tt*RuvC, 4LD0) also exhibited a central β sheet (Górecka *et al*, 2013). However, the overall structure is more distantly related to that of Mus81 compared to T7 endo.

Interestingly, hMus81 shares remarkable common features with 5′ nucleases such as hFEN1 (3Q8M, Tsutakawa *et al*, 2011) and Exo1 (3QE9, Orans *et al*, 2011) despite low (6-8%) sequence identity. The core of these proteins, a six-stranded sheet flanked by helices, shows less than 2.6 Å rms deviations for 77 ~ 87 Cα atoms. Helices α1 to α5 of hMus81 correspond well to the equivalent helices of hFEN1 and hExo1 (Fig 5A and Supplementary Fig S5A). Furthermore, three helices (α10, α11, and α12) in the key DNA-binding region (K^+ ion/H2TH) of hFEN1 are superimposed well onto the corresponding helices (α7, α8, and α9) of MHhH2 (Supplementary Fig S5B and C).

Importantly, Mus81 and 5′ nucleases share several conserved features associated with substrate recognition, DNA bending, and protein conformation change (Fig 5A and B). First, the hydrophobic wedge of 5′ flap nuclease, which separates pre- and post-nick dsDNA, is overlaid well with the wedge of hMus81-Eme1 (Grasby *et al*, 2012). Second, the "5′ end binding pocket" in hMus81-Eme1 resembles the 3′ flap binding site that interacts with a single nucleotide in 5′ flap nuclease. These striking similarities suggest that the structural conservations within the 5′ nuclease family members now extend to the Mus81/Eme1 nuclease/resolvase (Ciccia *et al*, 2008; Grasby *et al*, 2012). While the disorder-to-order transition occurs in the Eme1 linker that is far apart from the active site in Mus81-Eme1, the transition is observed in the helical arch which is located on top of the active site in FEN1 (Tsutakawa *et al*, 2011). Nevertheless, substrate-induced transitions are required for the substrate selection in both Mus81 and FEN1: FEN1 is believed to determine its substrates by controlling the entrance of the active site, whereas Mus81 achieves this by adjusting the position of 2HhH2 relative to nuclease. Fourth, both 5′ flap DNA in FEN1 and 3′ flap DNA in Mus81-Eme1 are sharply bent and exhibited a pseudo-mirror symmetrical relationship with their terminal bases unpaired (Fig 5B and C). By using the similar strategies, yet with pseudo-symmetrical features (5′ flap for 3′ flap binding pocket vs 3′ flap for 5′ end binding pocket), Mus81-Eme1 and FEN1 family nucleases resolve substrates with opposite flap.

Discussion

In this study, we have determined several Mus81-Eme1 structures that are bound to various flap DNA substrates. While the 3′ flap DNA is one of the best *in vitro* substrates for Mus81-Eme1, the 5′ flap DNA is not cleaved efficiently (Ehmsen & Heyer, 2008). Based on structural, biochemical, and biophysical data, we explained how Mus81-Eme1 recognizes and cleaves DNA substrates.

Conformational change reveals two essential features for substrate recognition and bending

Previously, structures of an apo Mus81-Eme1 and an archaeal XPF homologue suggested that the substrate DNA should be bent to place its incision strand to an active site (Newman *et al*, 2005; Chang *et al*, 2008). The present study confirms that dual

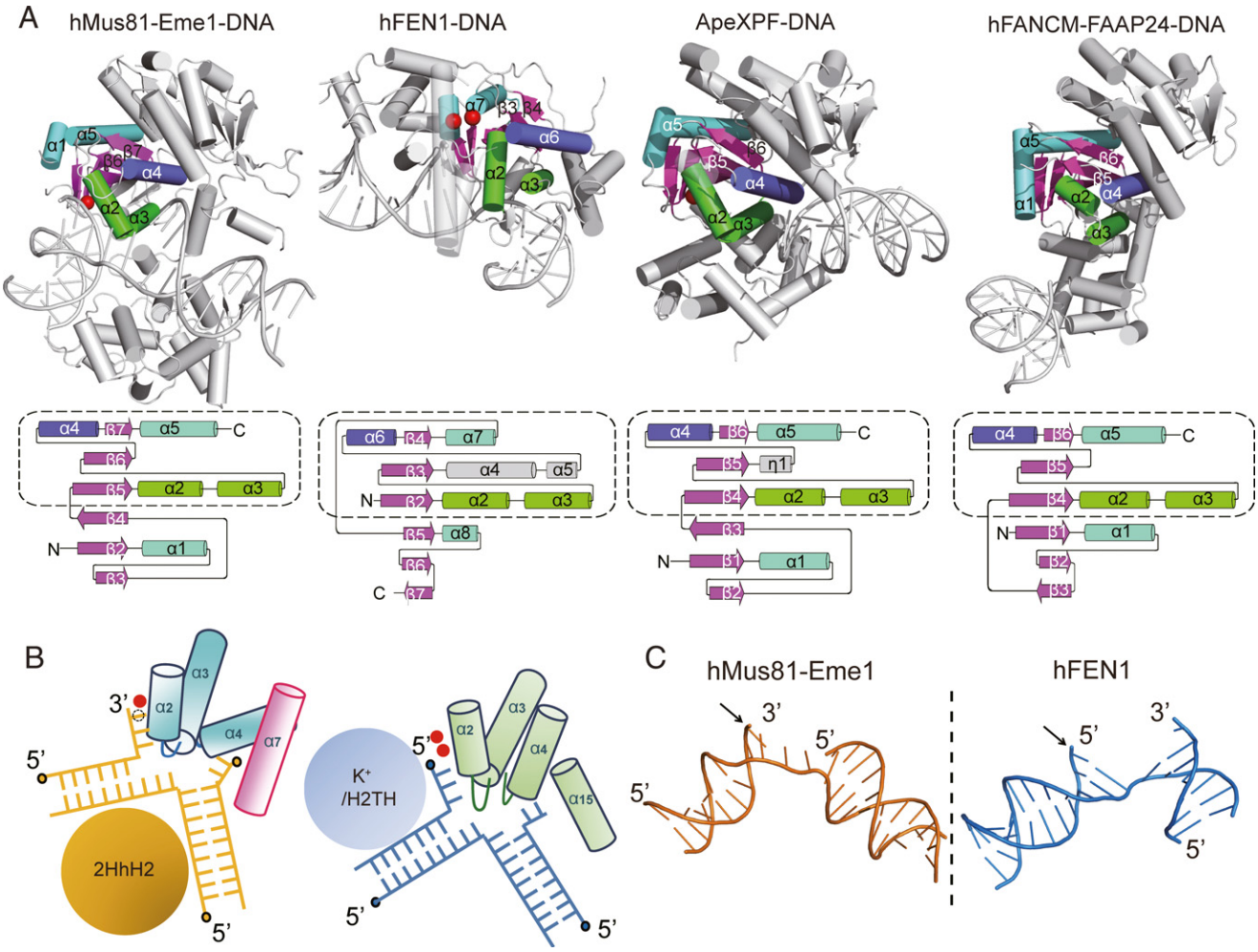

Figure 5. Comparison of the structures and topologies of hMus81-Eme1, hFEN1, ApXPF, and FANCM-FAAP24.

A Key features of hMus81-Eme1 (crystal II) including helices α2 and α3 (wedge) are in green, and helix α4 (pocket) is in blue. Equivalent strands are shown in magenta. Corresponding regions of hFEN1 (3QE9), ApXPF (2BGW), and FANCM-FAAP24 (4BXO) are also shown. Comparison of the topologies of hMus81-Eme1, hFEN1 is shown below. Topologically similar parts are boxed and painted with same color.

B Comparison of the key features in 3′ and 5′ flap endonuclease: Schematic models of the hMus81-Eme1 bound to the 3′ flap DNA (left) and the FEN1/hExo1—5′ flap DNA (right) are shown to highlight the common structural features.

C Structures of the 3′ flap DNA bound to hMus81-Eme1 (orange, left) and the 5′ flap DNA bound to FEN1 (blue, right) are shown. Both DNA substrates from a similar orientation of the proteins exhibit pseudo-mirror symmetry. An incision site is marked with an arrow.

recognition of a DNA substrate by both MHhH2 and EHhH2 domains together with the nuclease domain indeed kinks the 3′ flap DNA and guides the 3′ end of an incision strand to the active site. Importantly, we show that DNA bending cannot be achieved without significant conformational changes for Mus81-Eme1 from a closed to an open form (Fig 2A and B). Structure of crystal I suggests that initial binding of post-nick DNA is necessary and sufficient to induce structural transitions (Fig 1A and B). The substrate-induced disorder-to-order change of the Eme1 linker results in rotation of 2HhH2, which unmasks the hydrophobic wedge and creates the pocket (Fig 2B). Mutational analyses of the pocket and wedge suggest that only in the presence of these features, Mus81-Eme1 exhibited its full nuclease activities. Presence of similar wedge and pocket in the 5′ flap nucleases raises a possibility that these are universal features in the substrate recognition and bending in flap nuclease family members.

Basis for the preference of 3′ flap DNA to 5′ flap by Mus81-Eme1

Structure of crystal I revealed that a 5′ flap DNA forms duplex DNA, which resembles the post-nick duplex of the 3′ flap DNA bound to Mus81-Eme1. The presence of the 5′ end binding pocket suggests that such duplex DNA formation is not caused by serendipity. Because the 5′ end binding pocket cannot accommodate the long 5′ flap, the 5′ flap DNA binds to MHhH2 as an entity with its 5′ terminal nucleotide mimicking the 5′ nicked end of a 3′ flap DNA, thereby inducing the conformational change in Mus81-Eme1. Since the binding pocket is limited in its size and shape of the 5′ nicked

end, it is unlikely that DNA without a nick such as the 5′ flap, splayed arms, and intact JMs can effectively bind to the pocket, which is consistent with biochemical data (Boddy *et al*, 2001; Fricke *et al*, 2005; Ehmsen & Heyer, 2008).

Selection of the incision point on a substrate

Earlier studies showed that human and yeast Mus81-Eme1/Mms4 cleave two to seven nts upstream from the 5′ nicked (or junction) end of the JMs including 3′ flap substrate (Bastin-Shanower *et al*, 2003; Gaskell *et al*, 2007; Ciccia *et al*, 2008). Seven Mus81-Eme1-DNA structures between 2.8 ~ 6.5 Å allow us to postulate how Mus81-Eme1 determines the incision point of 3′ flap DNA substrate. Structures showed that (i) two 5′ terminal nucleotides (including a disordered nt) at 5′ flap DNA are unpaired (or two nts at 5′ nicked end of the post-nick duplex are unpaired) and (ii) a ssDNA with approximately 4 nts connects pre- and post-nick duplex of the 3′ flap DNA. Based on these results, we can predict the 3′ two nts of the pre-nick DNA are unpaired from a (3′ flap) branch point (crystals II and III, Fig 6A–C). We then placed the incision strand of a pre-nick DNA into the corresponding region of the 6 Å electron density map. When this structure is superimposed with that of crystal I (2.8 Å), the closest nucleotide ("-3 nt") from the Mg^{2+} site (approximately 4 Å) is located at three nt upstream from the branch point (Figs 4C, 6B and C). Also, "-3 nt" is at three nt upstream from the 5′ nicked end (or the "5′ end binding pocket"). Thus, the incision site would be equally distant from the binding pocket or from a branch point in our structure-based model, which suggests that either the branch point or the 5′ junction at the pocket can be used as a reference point. Recent studies report that it is the branch point, rather than 5′ junction that determines the incision site of substrates by budding yeast Mus81-Eme1, supporting our structure (Ehmsen & Heyer, 2009).

Insights into the junction resolving mechanism of Mus81-Eme1

Mus81-Eme1 is known to resolve nicked HJs or intact HJs both *in vitro* and *in vivo*. Structural basis of the selectivity of the 3′ flap over the 5′ flap DNA by Mus81-Eme1 can be extended to understand how Mus81-Eme1 participates in resolving JMs. Mus81-Eme1 is likely to recognize the nicked HJs over intact HJs through its 5′ end binding pocket. In addition, intact HJs have a significant restraint at a junction between arms and cannot be efficiently separated by the wedge. As a result, DNA bending that we have observed in the present study may not be efficiently achieved in intact HJs. However, once the nick is introduced, it would relieve the restraint at the junction between arms as well as generating the 5′ nicked end. Recent studies suggested that Slx1 primarily introduces the first nick to intact HJs in the MUS-SLX complex (Castor *et al*, 2013; Garner *et al*, 2013; Wyatt *et al*, 2013). Our structures suggest that an initial nick produced by Slx1 can be lodged into the pocket of Mus81-Eme1 for the second cleavage, which support the nick-and-counternick mechanism by MUS-SLX.

A model for the Mus81-Eme1—nicked JM complex

How does Mus81-Eme1 recognize the nicked JMs? Previous studies showed that mutations of Arg289, Arg293 (helix α1), Arg406, and Arg417 (helix α5) of Mus81 significantly decreased nuclease activities toward a nicked HJ and replication fork, while nuclease activities toward a 3′ flap DNA remained unaltered (Chang *et al*, 2008). The 6.0 Å electron density in crystal III revealed the trace for the crystallographic symmetry-related DNA at the surface, which is formed by helices α1 and α5 and loop β6-α4 (Fig 6D). Several basic residues are clustered in this region. This DNA trace can be extended from the pre-nick DNA, and together with the pre- and

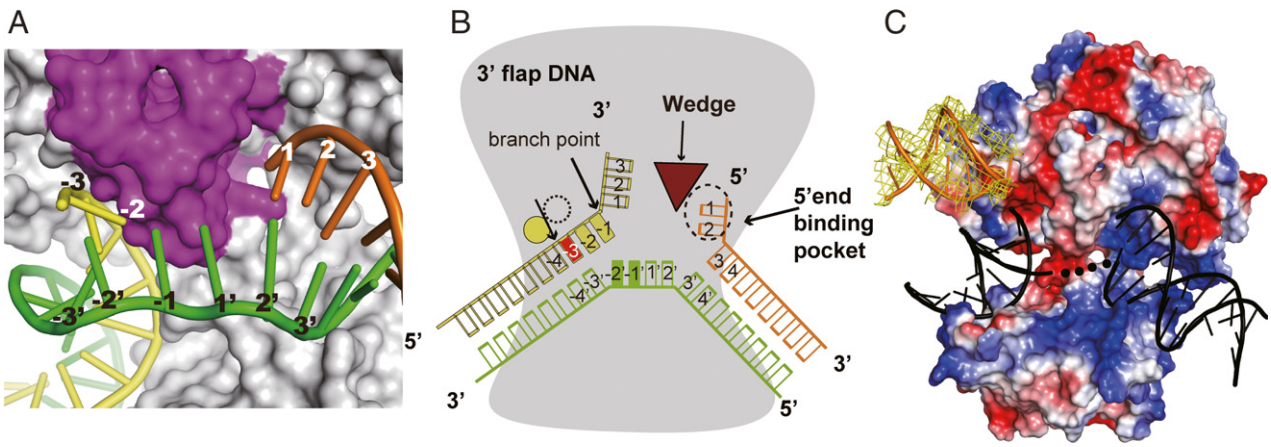

Figure 6. Schematic diagram representing the substrate recognition and incision model.

A Surface representation of the substrate binding at the active site of Mus81-Eme1. The figure is drawn from a crystal II (6.5 Å) structure. An incised and the 5′ nicked end of a 3′ flap DNA are shown in yellow and orange, respectively. The wedge is shown in purple. The nucleotides are numbered from a branch point of a 3′ flap (same as in (B)). Right and left from a branch point are labeled with positive and negative numbers, respectively.

B Schematic representation of the substrate recognition by Mus81-Eme1 from crystals II and III. The "-2" (yellow box) and "-3" (red box) terminal nucleotides are near the Mg^{2+} ion (yellow circle). A branch point is marked with an arrow. Another (putative) Mg^{2+} ion is in a dotted circle. The incision site within substrate is marked with an arrow.

C Surface representation of the substrate binding to hMus81-Eme1. Positively and negatively charged regions are shown in blue and red, respectively. A 3′ flap DNA is shown in black. A trace of a symmetry-related DNA is modeled in 6.0 Å electron density map (crystal III, yellow).

post-nick duplex, the overall DNA structure at the active site mimics a replication fork.

The linker between the nuclease and 2HhH2 domain is important for the substrate selectivity in MUS/XPF family members

Biologically, Mus81-Eme1 nuclease independently incises diverse substrates, while it could function as a JM resolvase in complex with Slx1-Slx4. As we have shown from the structural comparison analysis with 5′ nucleases, Mus81-Eme1 possesses several crucial features that can function as a flap nuclease. Consistent with this idea, in murine cells, the primary targets of Mus81-Eme1 in DNA interstrand cross-link repair are DNA molecules with structures other than intact HJs (Castor *et al*, 2013). The linker connecting the nuclease and 2HhH2 domains undergoes the most dramatic conformational change in response to DNA binding. This region in the MUS/XPF family members exhibits wide range of diversity in the length and composition (Supplementary Fig S2). As a result, the position of 2HhH2 relative to the nuclease domain in other MUS/XPF members is expected to be different from that of Mus81-Eme1. We predict that difference in the position of 2HhH2 confers the substrate selectivity to the MUS/XPF family nucleases. Structures of archaeal XPF homologue and FANCM-FAAP24 that consist of nuclease and HhH2 form markedly different architecture from that of Mus81-Eme, supporting this prediction (Fig 5A, Newman *et al*, 2005; Chang *et al*, 2008; Coulthard *et al*, 2013). In addition, residues that comprise the 5′ end binding pocket are conserved in Mus81 and Eme1, but not other members such as XPF, ERCC1, or FANCM. Nevertheless, it should be noted that an importance of 5′ end has been demonstrated for the archaeal XPF, which implicate the presence of "5′ end binding pocket" in XPF, possibly in other location (Roberts & White, 2005). Collectively, these results suggest that the substrate selectivity is achieved not only by the active site but also by differences in linker and location of 2HhH2 in MUS/XPF nucleases.

In conclusion, we have shown that the substrate-induced structural transition of Mus81-Eme1 provides critical features, which explain how this nuclease complex distinguishes the substrates. These structural features allow Mus81-Eme1 to function efficiently as a structure-selective nuclease by itself and as a resolvase for intact HJs together with other nucleases. Structures of the Mus81-Eme1 complex bound to flap DNA substrates presented here should provide insights into understanding the resolving mechanism of JM intermediates in HR repair and in the chromosome segregation.

Materials and Methods

Protein expression and purification

Genes encoding hMus81 (residues 246–551) and hEme1 (residues 178–570) were amplified by PCR and inserted into pCDF-duet and pET-duet, respectively. The *Escherichia coli* Rosetta (DE3) containing the two plasmids was grown in LB media. His-tagged hMus81-Eme1 was purified by a Ni^{2+}-NTA affinity chromatography. Fractions containing the hMus81-Eme1 complex were further purified using cation-exchange chromatography and dialyzed against a buffer containing 20 mM Bis-Tris-propane-HCl (BTP-HCl) pH 7.0, 0.2 M NaCl, and 5 mM DTT.

Crystallization and data collection

Crystals of the hMus81-Eme1-DNA complex were grown by the hanging drop vapor diffusion method at 4°C. Crystals (I) containing 17-bp 5′ flap DNA were grown with the crystallization buffer containing 5% ethanol, 0.1 M Tris–HCl, pH 7.0, and 5 mM DTT. Crystals (II) with a 32-bp 3′ flap DNA were grown from the buffer containing 16% methyl pentanediol (MPD), 0.1 M sodium acetate, pH 5.0, 20 mM hexammine-cobalt chloride, and 5 mM DTT. Crystals (III) with 24-bp 3′ flap DNA were obtained from the buffer containing 13% butanediol, 0.1 M sodium acetate, pH 5.0, and 5 mM DTT. For Mg^{2+}-bound crystals (crystal I), crystals were soaked in crystallization buffer containing 1 mM $MgCl_2$ for 5 days. Diffraction data from the hMus81-Eme1-DNA crystals were collected at −170°C, either at the Pohang Accelerator Light Source or at 0.9795 Å at the Structural Biology Center (SBC) ID beamline (sector 19) at the Advanced Photon Source. Diffraction data were integrated and scaled using the HKL3000 package (Otwinowski & Minor, 1997; Supplementary Table S1).

Structure determination and refinement

The structure of the hMus81-Eme1-DNA complex was determined by the molecular replacement method. For crystal I, we initially determined the position of the nuclease: nuclease-like domain of hMus81-Eme1 using the nuclease: nuclease-like domain of the zfMus81-hEme1 structure (2ZIU), followed by locating the 2HhH2 domain. After density modification, an electron density map generated at a resolution of 2.8 Å using the PHENIX program (Adams *et al*, 2010) clearly revealed positions for Mus81 and Eme1 linkers and the DNA molecule, which allowed us to trace most chains. Successive rounds of model building using COOT (Emsley & Cowtan, 2004) and refinement using PHENIX were performed to build the complete model. A Mg^{2+} ion was identified from difference Fourier map generated at a resolution of 2.85 Å. The structure of this hMus81-Eme1 was then used to determine the positions of the nuclease and 2HhH2 domains in crystals II and III with the program PHASER (McCoy *et al*, 2007). The molecular replacement model of two hMus81-Eme1 protomers in the asymmetric unit (crystal II) or four hMus81-Eme1 protomers (crystal III) was improved by rigid body refinement using five rigid groups per protomer and by TLS refinement using five TLS groups per protomer with the program PHENIX (Adams *et al*, 2010). The twofold ncs (crystal II) or fourfold ncs averaged map (crystal III) of the nuclease complex model clearly revealed the density for the substrate including the pre- and post-nick duplex DNA regions. For pre-nick and post-nick duplex, a model of an ideal B-type DNA and a DNA model from crystal I was positioned into a map, respectively. The model was further improved by rigid body refinement with a twofold ncs restraint for crystal II or a fourfold ncs restraint for crystal III and with a 2.8 Å structure of hMus81-Eme1 as reference model restraints.

Nuclease activity assay

A cleavage reaction mixture containing 20 nM ^{32}P-labeled nHJ and 3′ flap DNA substrate in reaction buffer (25 mM Tris–HCl, pH 8.0, 5 mM β-mercaptoethanol, 100 μg/ml bovine serum albumin (Sigma-Aldrich, USA), 5% glycerol, and 10 mM $MgCl_2$) was incubated for various time period (2–60 min) at 37°C. The reaction

was stopped by incubation with 1× reaction stop buffer (0.3% SDS, 5 mM EDTA, pH 8.0, and 0.1 mg/ml proteinase K (Sigma-Aldrich, USA)), for 30 min at 37°C. The products were resolved in a 10% native polyacrylamide gel in 1× TBE (Tris-borate-EDTA). The products were separated for 90 min at 13/Vcm. Uncleaved substrates were quantified by a phosphorimager analysis using MultiGauge version 3.0 (Fujifilm).

Supplementary information for this article is available online: http://emboj.embopress.org

Acknowledgments

We thank Phil Jeffrey, Sang UK Kim and Chang Il Ban for helpful discussion. We also thank G-One Ahn for critical reading. We also thank Wolf-Dietrich Heyer for sharing unpublished results (The Mus81-Mms4 structure-selective endonuclease requires nicked DNA junctions to undergo conformational changes and bend its DNA substrates for cleavage, Mukherjee *et al*, Nucleic Acids Res. In press). This work was supported by grants from the National R&D Program for Cancer Control, Ministry for Health and Welfare (1020280), National Research Foundation of Korea (NRF) grant funded by the Korea government (MEST, No. 2012004028, No. 2012-054226, and No. 20120008833), a rising star program (POSTECH), and the BK21 program (Ministry of Education). The authors declare that none of the authors have a financial interest related to this work. Coordinates and structure factors have been deposited to RCSB (4P0P for the 2.8 Å complex, 4 P0Q for the 2.85 Å metal-free complex, 4P0R for the 6.5 Å complex, 4P0S for the 6.0 Å complex).

Author contributions

G-HG conducted the experiments with the help of AJ and YF; G-HG and AJ carried out crystallization; G-HG, KB, YK, and YC performed structure determination; G-HG, KB, YK, AJ, and YC participated in experimental design and data analysis; YC conceived of the project and wrote the paper.

Conflict of interest

The authors declare that they have no conflict of interest.

References

Abraham J, Lemmers B, Hande MP, Moynahan ME, Chahwan C, Ciccia A, Essers J, Hanada K, Chahwan R, Khaw AK (2003) Eme1 is involved in DNA damage processing and maintenance of genomic stability in mammalian cells. *EMBO J* 22: 6137 – 6147

Adams PD, Afonine PV, Bunkóczi G, Chen VB, Davis IW, Echols N, Headd JJ, Hung LW, Kapral GJ, Grosse-Kunstleve RW, McCoy AJ, Moriarty NW, Oeffner R, Read RJ, Richardson DC, Richardson JS, Terwilliger TC, Zwart PH (2010) PHENIX: a comprehensive Python-based system for macromolecular structure solution. *Acta Crystallogr D* 66: 213 – 221

Bastin-Shanower SA, Fricke WM, Mullen JR, Brill SJ (2003) The mechanism of Mus81-Mms4 cleavage site selection distinguishes it from the homologous endonuclease Rad1-Rad10. *Mol Cell Biol* 23: 3487 – 3496

Boddy MN, Gaillard PH, McDonald WH, Shanahan P, Yates JR 3rd, Russell P (2001) Mus81-Eme1 are essential components of a Holliday junction resolvase. *Cell* 107: 537 – 548

Castor D, Nair N, Déclais AC, Lachaud C, Toth R, Macartney TJ, Lilley DM, Arthur JS, Rouse J (2013) Cooperative Control of Holliday junction resolution and DNA repair by the SLX1 and MUS81-EME1 Nucleases. *Mol Cell* 52: 221 – 233

Cejka P, Plank JL, Bachrati CZ, Hickson ID, Kowalczykowski SC (2010) Rmi stimulates decatenation of double Holliday junctions during dissolution by Sgs1-Top3. *Nat Struct Mol Biol* 17: 1377 – 1382

Chang JH, Kim JJ, Choi JM, Lee JH, Cho Y (2008) Crystal structure of the Mus81-Eme1 complex. *Genes Dev* 22: 1093 – 1106

Chen XB, Melchionna R, Denis CM, Gaillard PH, Blasina A, Van WI, Boddy MN, Russell P, Vialard J, McGowan CH (2001) Human Mus81-associated endonuclease cleaves Holliday junctions *in vitro*. *Mol Cell* 8: 1117 – 1127

Ciccia A, McDonald N, West SC (2008) Structural and functional relationships of the XPF/MUS81 family of proteins. *Annu Rev Biochem* 77: 259 – 287

Constantinou A, Chen XB, McGowan CH, West SC (2002) Holliday junction resolution in human cells: two junction endonucleases with distinct substrate specificities. *EMBO J* 21: 5577 – 5585

Coulthard R, Deans AJ, Swuec P, Bowles M, Costa A, West SC, McDonald NQ (2013) Architecture and DNA recognition elements of the Fanconi anemia FANCM-FAAP24 complex. *Structure* 21: 1648 – 1658

Deans AJ, West SC (2011) DNA interstrand crosslink repair and cancer. *Nat Rev Cancer* 11: 467 – 480

Dendouga N, Gao H, Moechars D, Janicot M, Vialard J, McGowan CH (2005) Disruption of murine Mus81 increases genomic instability and DNA damage sensitivity but does not promote tumorigenesis. *Mol Cell Biol* 25: 7569 – 7579

Doe CL, Ahn JS, Dixon J, Whitby MC (2002) Mus81-Eme1 and Rqh1 involvement in processing stalled and collapsed replication forks. *J Biol Chem* 277: 32753 – 32759

Ehmsen KT, Heyer WD (2008) Saccharomyces cerevisiae Mus81-Mms4 is a catalytic, DNA structure-selective endonuclease. *Nucleic Acids Res* 36: 2182 – 2195

Ehmsen KT, Heyer WD (2009) A junction branch point adjacent to a DNA backbone nick directs substrate cleavage by Saccharomyces cerevisiae Mus81-Mms4. *Nucleic Acids Res* 37: 2026 – 2036

Emsley P, Cowtan K (2004) Coot: model-building tools for molecular graphics. *Acta Crystallogr D* 60: 2126 – 2132

Fekairi S, Scaglione S, Chahwan C, Taylor ER, Tissier A, Coulon S, Dong MQ, Ruse C, Yates JR 3rd, Russell P (2009) Human SLX4 is a Holliday junction resolvase subunit that binds multiple DNA repair/recombination endonucleases. *Cell* 138: 78 – 89

Freudenthal BD, Beard WA, Shock DD, Wilson SH (2013) Observing a DNA polymerase choose right from wrong. *Cell* 154: 157 – 168

Fricke WM, Bastin-shanower SA, Brill SJ (2005) Substrate specificity of the Saccharomyces cerevisiae Mus81-Mms4 endonuclease. *DNA Repair (Amst)* 4: 243 – 251

Gaillard PH, Noguchi E, Shanahan P, Russell P (2003) The endogenous Mus81-Eme1 complex resolves Holliday junctions by a nick and counternick mechanism. *Mol Cell* 12: 747 – 759

Garner E, Kim Y, Lach FP, Kottemann MC, Smogorzewska A (2013) Human GEN1 and the SLX4-Associated Nucleases MUS81 and SLX1 are essential for the resolution of replication-induced Holliday junctions. *Cell Rep* 5: 1 – 9

Gaskell LJ, Osman F, Gilbert RJ, Whitby MC (2007) Mus81 cleavage of Holliday junctions: a failsafe for processing meiotic recombination intermediates? *EMBO J* 26: 1891 – 1901

Górecka KM, Komorowska W, Nowotny M (2013) Crystal structure of RuvC resolvase in complex with Holliday junction substrate. *Nucleic Acids Res* 41: 9945 – 9955

Grasby JA, Finger LD, Tsutakawa SE, Atack JM, Tainer JA (2012) Unpairing and gating: sequence-independent substrate recognition by FEN superfamily nucleases. *Trends Biochem Sci* 37: 74 – 84

Hadden JM, Déclais AC, Carr SB, Lilley DM, Phillips SE (2007) The structural basis of holliday junction resolution by T7 endonuclease 1. *Nature* 449: 621 – 624

Hanada K, Budzowska M, Davies SL, Drunen E, Onizawa H, Beverloo HB, Maas A, Essers J, Hickson ID, Kanaar R (2007) The structure-selective endonuclease Mus81 contributes to replication restart by generating double-strand DNA breaks. *Nat Struct Mol Biol* 14: 1096 – 1104

Hanada K, Budzowska M, Modesti M, Maas A, Wyman C, Essers J, Kanaar R (2006) The structure-specific endonuclease Mus81-Eme1 promotes conversion of interstrand DNA crosslinks into double-strands breaks. *EMBO J* 25: 4921 – 4932

Hiyama T, Katsura M, Yoshihara T, Ishida M, Kinomura A, Tonda T, Asahara T, Miyagawa K (2006) Haploinsufficiency of the Mus81-Eme1 endonuclease activates the intra-S-phase and G2/M checkpoints and promotes rereplication in human cells. *Nucleic Acids Res* 34: 880 – 892

Hollingsworth NM, Brill SJ (2004) The Mus81 solution to resolution: generating meiotic crossovers without Holliday junctions. *Genes Dev* 18: 117 – 125

Interthal H, Heyer WD (2000) MUS81 encodes a novel helix-hairpin-helix protein involved in the response to UV- and methylation-induced DNA damage in Saccharomyces cerevisiae. *Mol Gen Genet* 263: 812 – 827

Ip SC, Rass U, Blanco MG, Flynn HR, Skehel JM, West SC (2008) Identification of Holliday junction resolvases from humans and yeast. *Nature* 456: 357 – 361

McCoy AJ, Grosse-Kunstleve RW, Adams PD, Winn MD, Storoni LC, Read RJ (2007) Phaser crystallographic software. *J Appl Cryst* 40: 658 – 674

Muñoz IM, Hain K, Déclais AC, Gardiner M, Toh GW, Sanchez-Pulido L, Heuckmann JM, Toth R, Macartney T, Eppink B, Kanaar R, Ponting CP, Lilley DM, Rouse J (2009) Coordination of structure-selective nucleases by human SLX4/BTBD12 is required for DNA repair. *Mol Cell* 35: 116 – 127

Naim V, Wilhelm T, Debatisse M, Rosselli F (2013) ERCC1 and MUS81-EME1 promote sister chromatid separation by processing late replication intermediates at common fragile sites during mitosis. *Nat Cell Biol* 8: 1008 – 1015

Newman M, Murray-Rust J, Lally J, Rudolf J, Fadden A, Knowles PP, White MF, McDonald NQ (2005) Structure of an XPF endonuclease with and without DNA suggests a model for substrate recognition. *EMBO J* 24: 895 – 905

Nishino T, Komori K, Ishino Y, Morikawa K (2005) Structural and functional analyses of an archaeal XPF/Rad1/Mus81 nuclease: asymmetric DNA binding and cleavage mechanisms. *Structure* 13: 1183 – 1192

Orans J, McSweeney EA, Iyer RR, Hast MA, Hellinga HW, Modrich P, Beese LS (2011) Structures of human exonuclease 1 DNA complexes suggest a unified mechanism for nuclease family. *Cell* 145: 212 – 223

Otwinowski Z, Minor W (1997) Processing of X-ray diffraction data collected in oscillation mode. *Methods Enzymol* 276: 307 – 326

Roberts JA, White MF (2005) DNA end-directed and processive nuclease activities of the archaeal XPF enzyme. *Nucleic Acids Res* 33: 6662 – 6670

Schwartz EK, Heyer WD (2011) Processing of joint molecule intermediates by structure-selective endonucleases during homologous recombination in eukaryotes. *Chromosoma* 120: 109 – 127

Svendsen JM, Smogorzewska A, Sowa ME, O'Connell BC, Gygi SP, Elledge SJ, Harper JW (2009) Mammalian BTBD12/SLX4 assembles a Holliday junction resolvase and is required for DNA repair. *Cell* 138: 63 – 77

Tsodikov OV, Enzlin JH, Scharer OD, Ellenberger T (2005) Crystal structure and DNA binding functions of ERCC1, a subunit of the DNA structure-specific endonuclease XPF-ERCC1. *Proc Natl Acad Sci* 102: 11236 – 11241

Tsutakawa SE, Classen S, Chapados BR, Arvai AS, Finger LD, Guenther G, Tomlinson CG, Thompson P, Sarker AH, Shen B, Cooper PK, Grasby JA, Tainer JA (2011) Human flap endonuclease structures, DNA double-base flipping, and a unified understanding of the FEN1 superfamily. *Cell* 145: 198 – 211

Wechsler T, Newman S, West SC (2011) Aberrant chromosome morphology in human cells defective for Holliday junction resolution. *Nature* 471: 642 – 646

Whitby MC, Osman F, Dixon J (2003) Cleavage of model replication forks by fission yeast Mus81-Eme1 and budding yeast Mus81-Mms4. *J Biol Chem* 278: 6928 – 6935

Wu L, Hickson ID (2003) The Bloom's syndrome helicase suppresses crossing over during homologous recombination. *Nature* 426: 870 – 874

Wyatt HD, Sarbajna S, Matos J, West SC (2013) Coordinated Actions of SLX1-SLX4 and MUS81-EME1 for Holliday junction resolution in Human Cells. *Mol Cell* 52: 1 – 14

Yang W (2008) An equivalent metal ion in one- and two-metal-ion catalysis. *Nat Struct Mol Biol* 15: 1228 – 1231

Yang W, Lee JY, Nowotny M (2006) Making and breaking nucleic acids: two-Mg^{2+}-ion catalysis and substrate specificity. *Mol Cell* 22: 5 – 13

Ying S, Minocherhomji S, Chan KL, Palmai-Pallag T, Chu WK, Wass T, Mankouri HW, Liu Y, Hickson ID (2013) MUS81 promotes common fragile site expression. *Nat Cell Biol* 15: 1001 – 1007

